One-Step Ahead Prediction of Angular Momentum about the Contact Point for Control of Bipedal Locomotion: Validation in a LIP-inspired Controller

Yukai Gong and Jessy Grizzle

***Abstract*— Ultimately, feedback control is about making adjustments using current state information in order to meet an objective in the future. In the control of bipedal locomotion, linear velocity of the center of mass has been widely accepted as the primary variable around which feedback control objectives are formulated. In this paper, we argue that it is easier to predict the one-step ahead evolution of angular momentum about the contact point than it is to make a similar prediction for linear velocity, and hence it provides a superior quantity for feedback control. So as not to confuse the benefits of predicting angular momentum with any other control design decisions, we reformulate the standard LIP model in terms of angular momentum and show how to regulate swing foot touchdown position at the end of the current step so as to meet an angular momentum objective at the end of the next step. We implement the resulting feedback controller on the 20 degree-of-freedom bipedal robot, Cassie Blue, where each leg accounts for nearly one-third of the robot's total mass of 32 Kg. Under this controller, the robot achieves fast walking, rapid turning while walking, large disturbance rejection, and locomotion on rough terrain.**

I. Introduction

Maintaining "balance" is widely viewed as the most critical problem in bipedal locomotion. The notion of "balance" needs to be quantified so that it can be transformed into a feedback control objective. Some represent "balance" with an asymptotically stable periodic orbit [1], [2]. A common approach is to summarize the status of a nonlinear high-dimensional robot model with a few key variables. The most frequently proposed variables as surrogates for "balance" include Center of Mass (COM) velocity [3]–[7], COM position [8], Capture Point [9], [10], Zero Moment Point [11], [12], and Angular Momentum [13], [14].

In this paper we choose angular momentum about the contact point as our primary control variable. Some of its desirable properties in bipedal locomotion have been highlighted and exploited for feedback control in [13]–[17]. We choose to demonstrate our results by reformulating the well-known Linear Inverted Pendulum (LIP) model [18] in terms of angular momentum about the contact point. We emphasize that the LIP model, when reformulated in terms of angular momentum, has higher fidelity when applied to realistic robot models, than when based on linear velocity. Powell and Ames [14] developed a similarly reformulated LIP model and they chose to regulate the angular momentum at the beginning of the next step through touch down timing and transfer of momentum at impact. Here we take advantage of the higher fidelity of predicted angular momentum about the contact point and choose to regulate it at the end of next step, which can then be more effectively controlled by foot placement [19], [20].

To demonstrate that our results transfer in practice to a realistic bipedal robot, we implement the resulting feedback controller on the 20 degree-of-freedom bipedal robot, Cassie Blue, where each leg accounts for nearly one-third of the robot's total mass of 32 Kg. In experiments, Cassie Blue is able to execute walking in a straight line up to 2.1 m/s, simultaneously walking forward and diagonally on grass at 1 m/s, make quick, sharp turns, and handle very challenging undulating terrain. For the purpose of completeness, we note that a LIP-inspired controller organized around COM velocity has been implemented on a Cassie-series robot in [21].

The main contributions of the paper are as follows:

- Demonstrate that the one-step-ahead prediction of angular momentum about the contact point provided by a LIP model is superior to a one-step-ahead prediction of linear velocity of the center of mass when applied to realistic robots;
- Formulate a foot placement strategy based on the one-step-ahead prediction of angular momentum.
- Demonstrate the resulting controller can achieve highly dynamic gaits on a 3D bipedal robot with legs that are far from massless; see Fig. 1

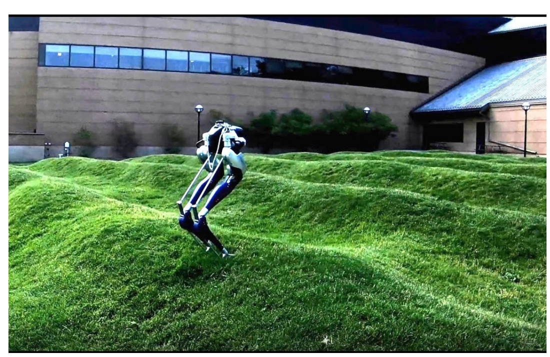

Fig. 1: Cassie Blue, by Agility Robotics, on the iconic University of Michigan Wave Field.

Funding for this work was provided in part by the Toyota Research Institute (TRI) under award number No. 02281 and in part by NSF Award No. 1808051. All opinions are those of the authors.

The authors are with the College of Engineering and the Robotics Institute, University of Michigan, Ann Arbor, MI 48109 USA {ykgong,grizzle}@umich.edu

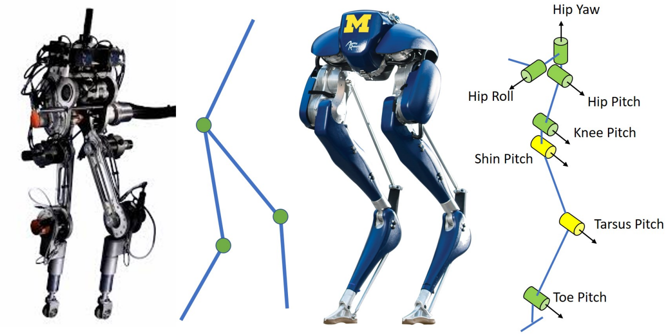

Fig. 2: Rabbit and Cassie. Rabbit is planar robot with 2 joints on each leg and Cassie is 3D robot with 7 joints on each leg.

We will use both Rabbit [22] and Cassie Blue to illustrate our developments in the paper. Experiments will be conducted exclusively on Cassie. Rabbit is a 2D biped with five links, four actuated joints, and a mass of 32 Kg; see Fig. 2. Each leg weighs 10 kg, with 6.8 kg on each thigh and 3.2 kg on each shin.

The bipedal robot shown in Fig. 1, named Cassie Blue, is designed and built by Agility Robotics. The robot weighs 32kg. It has 7 deg of freedom on each leg, 5 of which are actuated by motors and 2 are constrained by springs; see Fig. 2. A floating base model of Cassie has 20 degrees of freedom. Each foot of the robot is blade-shaped and provides 5 holonomic constraints when it is on ground. Though each of Cassie's legs has approximately 10 kg of mass, most of the mass is concentrated on the upper part of the leg. In this regard, the mass distribution of Rabbit is a bit more typical of bipedal robots, which is why we include the Rabbit model in the paper.

The remainder of the paper is organized as follows. Section II and III introduce angular momentum and the LIP model. In Section IV, we show how to predict the evolution of angular momentum with a LIP model and how to use the prediction to decide foot placement. This provides a feedback controller that will stabilize a 3D LIP. In Section V, we provide our path to implementing the controller on Cassie Blue. Additional reference trajectories are required beyond a path for the swing foot, and we provide "an intuitive" method for their design. Section VI shows the experiment results. Conclusion are give in Sect. VII.

II. Angular Momentum About Contact Point

In the following, we will address two questions: why we can replace linear momentum with angular momentum for the design of feedback controllers and what are the benefits of doing so.

Initially, we address the *single support* phase of walking, meaning only one leg is in contact with the ground. Moreover, we are considering a point contact.

Let L denote the **angular momentum** about the contact point of the stance leg. The relationship between angular momentum and **linear momentum** for a 3D bipedal robot is

$$L = L_{\mathrm{CoM}} + p \times m_{\mathrm{tot}} v_{\mathrm{CoM}}, \tag{1}$$

where L_{CoM} is the angular momentum about the center of mass, v_{CoM} is the linear velocity of the center of mass, m_{tot} is the total mass of the robot, and p is the vector emanating from the contact point to the center of mass.

For a bipedal robot that is walking instead of doing somersaults, the angular momentum about the center of mass must oscillate about zero. Hence, (1) implies that the difference between L and $p \times m v_{\mathrm{CoM}}$ also oscillates around zero, which we will write as

$$L - p \times m_{\mathrm{tot}} v_{\mathrm{CoM}} = L_{\mathrm{CoM}} \text{ oscillates about } 0. \tag{2}$$

From (2), we see that we approximately obtain a desired linear velocity by regulating L.

The discussion so far has focused on a single support phase of a walking gait. Bipedal walking is characterized by the transition between left and right legs as they alternately take on the role of stance leg (aka support leg) and swing leg (aka non-stance leg). In double support, the transfer of angular momentum between the two contact points satisfies

$$L_2 = L_1 + p_{2\to 1} \times m_{\mathrm{tot}} v_{\mathrm{CoM}} \tag{3}$$

where L_i is the angular momentum about contact point i and $p_{1\to 2}$ is the vector from contact point 1 to contact point 2.

Hence, one can replace the control of linear velocity with control of angular momentum about the contact point. **But what are the advantages?**

(a) The first advantage of controlling L is that it provides a more comprehensive representation of current walking status by including both L_{CoM} and $p \times m v_{\mathrm{CoM}}$, between which momentum transfers forth and back during a step.

(b) Secondly, L has a relative degree three with respect to motor torques, if ankle torque is zero. Indeed, in this case,

$$\dot{L} = p \times m_{\mathrm{tot}} g. \tag{4}$$

where g is the gravitational constant. Consequently, L is very weakly affected by peaks in motor torque that often occur in off nominal conditions. Moreover, if a limb, such as the swing leg, is moving quickly in response to a disturbance, it will strongly affect the angular momentum about the center of mass and the robot's linear velocity, while leaving the angular momentum about the contact point only weakly affected.

(c) Thirdly, $\dot{L}$ is ONLY a function of the center of mass position, making it easy to predict its trajectory over a step.

(d) Finally, angular momentum about a given contact point is invariant under impacts at that point, and the change of angular momentum between two contact points depends only on the vector defined by the two contact points and the CoM velocity. Hence, we can easily determine the angular momentum about the new contact point by (3) when impact happens without approximating assumptions about the impact model. Moreover, if the vertical component of the $v_{\rm CoM}$ is zero and the ground is level, then $p_{2\to 1} \times m_{\rm tot} v_{\rm CoM} = 0$ and hence $L_2 = L_1$.

Figure 3 shows simulation plots of L, $L_{\rm CoM}$, and $v^x_{\rm CoM}$ for the planar bipedal robot, Rabbit, and the 3D bipedal robot, Cassie Blue. It is seen that the angular momentum about the contact point has the advantages discussed above.

III. One-Step-Ahead Prediction of Angular Momentum with the Linear Inverted Pendulum Model

This section introduces the Linear Inverted Pendulum (LIP) model of Kajita et al. [18] and the reformulation. The LIP model assumes the center of mass moves in a plane, the angular momentum about the center of mass is constant, and the legs are massless. Here, we will express the model in terms of its original coordinates, namely position and linear velocity of the center of mass, and in terms of the proposed new coordinates, namely position and angular momentum about the contact point. The dynamics of the inverted pendulum are exactly linear. Moreover, the 3D dynamics in the x and y directions are decoupled, and hence we only need to consider a $2D$ pendulum.

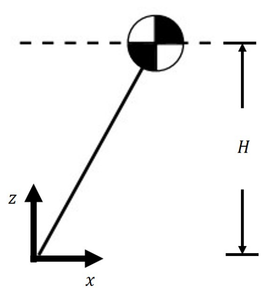

Fig. 4: Linear Inverted Pendulum Model. A prismatic joint in the leg allows the CoM to move along a given line.

Let H denote the height of the center of mass. For a 2D model, the dynamics in the x direction is

$$\begin{bmatrix} \dot{x} \\ \ddot{x} \end{bmatrix} = \begin{bmatrix} 0 & 1 \\ g/H & 0 \end{bmatrix} \begin{bmatrix} x \\ \dot{x} \end{bmatrix}, \tag{5}$$

where x is the position of CoM in the frame of contact point. if we assume there is no ankle torque. The solution of this linear system is

$$\begin{bmatrix} x(T) \\ \dot{x}(T) \end{bmatrix} = \begin{bmatrix} \cosh(\ell(T-t)) & 1/\ell \sinh(\ell(T-t)) \\ \ell \sinh(\ell(T-t)) & \cosh(\ell(T-t)) \end{bmatrix} \begin{bmatrix} x(t) \\ \dot{x}(t) \end{bmatrix}, \tag{6}$$

where $\ell = \sqrt{\frac{g}{H}}$, t is the current time and T is the (predicted) time of the end of the step.

We assume the body is a point mass and is moving on a horizontal plane, that is the height of the center of mass is constant. Because we are assuming a point mass, the angular momentum about the center of mass is zero. We now replace the states $\{x, \dot{x}\}$ with $\{x, L^y\}$, where L^y is the y-component of angular momentum about the contact point. The corresponding dynamic model is

$$\begin{bmatrix} \dot{x} \\ \dot{L}^y \end{bmatrix} = \begin{bmatrix} 0 & 1/mH \\ mg & 0 \end{bmatrix} \begin{bmatrix} x \\ L^y \end{bmatrix}, \tag{7}$$

and its corresponding solution is

$$\begin{bmatrix} x(T) \\ L^y(T) \end{bmatrix} = \begin{bmatrix} \cosh(\ell(T-t)) & 1/mH\ell \sinh(\ell(T-t)) \\ mH\ell \sinh(\ell(T-t)) & \cosh(\ell(T-t)) \end{bmatrix} \begin{bmatrix} x(t) \\ L^y(t) \end{bmatrix}, \tag{8}$$

where t is the current time and T is the (predicted) time of the end of the step.

For a point-mass inverted pendulum, where the mass moves on a horizontal plane, representations (5) and (7) are exactly the same. **So what have we gained? Importantly, for a real robot, where the two representations are only approximate, the second one is better for making predictions on the robot's state**, as we discussed in Sec. II.

Figure 5 compares the predictions of linear velocity and angular velocity about the contact point for a seven degree of freedom 2D model of Rabbit and a 20 degree of freedom 3D model of Cassie. In the figure, the simulated instantaneous values of $v^x_{\rm CoM}(t)$ and $L^y(t)$ are shown in blue. The red line shows the evolution of the predicted values at the end of a step for $v^x_{\rm CoM}(t)$ and $L^y(t)$ from (6) and (8). In a perfect predictor, the predicted values would be straight lines. It is clear that, when extrapolated to a realistic model of a robot, the prediction of angular momentum about the contact point is significantly more reliable than the estimate of linear velocity.

IV. High-Level Control Strategy in Terms of Angular Momentum

Because of the advantages of angular momentum versus linear velocity that we listed in Sect. III, we will use angular momentum about the contact point as the primary control variable. In this section, we explain our method for deciding where to end one step by initiating contact between the ground and the swing foot, thereby beginning the next step. In robot locomotion control, this is typically called "foot placement control".

A. Notation

We need to distinguish among the following time instances when specifying the control variables.

- T is the step time.
- T_k is the time of the kth impact.
- T_k^- is the end time of step k, so that
- T_k^+ is the beginning time of step $k+1$ and T_{k+1}^- is the end time of step $k+1$.
- $(T_k^- - t)$ is the time until the end of step k.

The superscripts $+$ and $-$ on T_k are due to the impact map; see [16].

- $p_{\rm st\to CoM}$, $p_{\rm sw\to CoM}$. Vector emanating from stance/swing foot to CoM. Here, the stance foot can be thought of as the current contact point and the swing foot is defining the of contact for the next impact and hence will be a control variable.

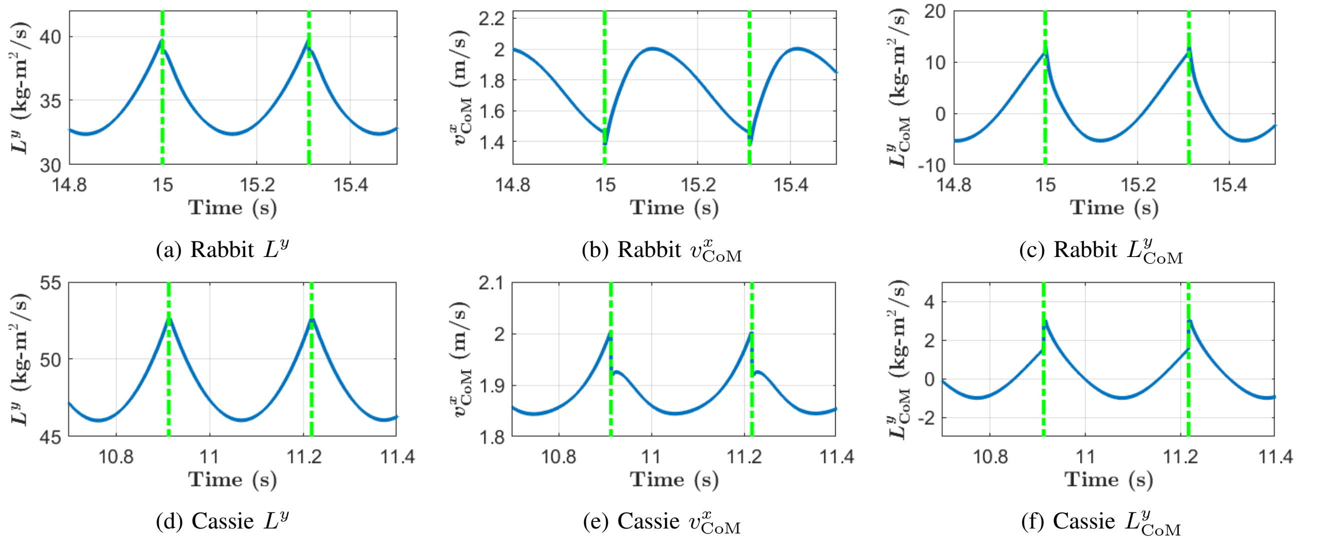

(a) Rabbit L^y (b) Rabbit v^x_{CoM} (c) Rabbit L^y_{CoM}

(d) Cassie L^y (e) Cassie v^x_{CoM} (f) Cassie L^y_{CoM}

Fig. 3: Comparison of L^y, L^y_{CoM}, v^x_{CoM} in simulation for the bipedal robots Rabbit and Cassie, while v^z_{CoM} is carefully regulated to zero. The angular momentum about the contact point, L^y, has a convex trajectory, both of which are similar to the trajectory of a LIP model, while the trajectory of the longitudinal velocity of the center of mass, v^x_{CoM}, has no particular shape. The variation of L_{CoM} throughout a step, which is caused by the legs of the robot having mass, is what leads to a difference in the COM velocity between a real robot and a LIP model. In this figure, L^y is continuous at impact, which is based on two conditions: $v^z_{\text{CoM}} = 0$ at impact and the ground is level. Even when these two conditions are not met, the jump in L at impact can be easily calculated with (3).

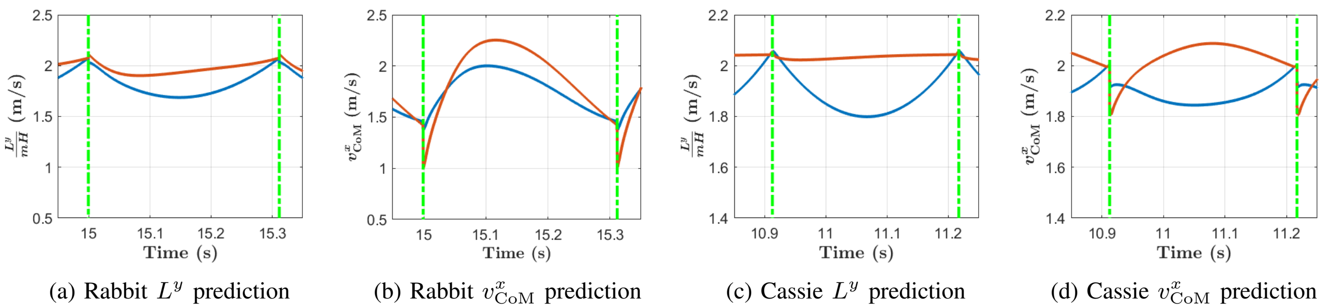

(a) Rabbit L^y prediction (b) Rabbit v^x_{CoM} prediction (c) Cassie L^y prediction (d) Cassie v^x_{CoM} prediction

Fig. 5: Comparison of the ability to predict velocity vs angular momentum at the end of a step. The instantaneous values are shown in blue and the predicted value at end of step is shown in red. The most crucial decision in the control of a bipedal robot is where to place the next foot fall. In the standard LIP controller, the decision is based on predicting the longitudinal velocity of the center of mass. In Sect. III we use angular momentum about the contact point. We do this because on realistic bipeds, the LIP model provides a more accurate and reliable prediction of L than v_{CoM}. The comparison is more significant on Rabbit, whose leg center of mass is further away from the overall CoM.

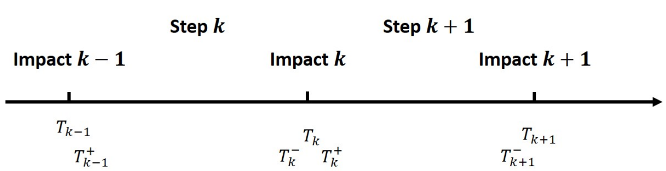

Fig. 6: Definition of T_k

B. Foot placement in longitudinal direction

In the following, we breakdown the estimated evolution of L^y from t to T^-_{k+1}, at three key time intervals or instances:

1) From t to T^-_k: From the second row of (8), an estimate for the angular momentum about the contact point at the end of current step, $\widehat{L}^y(T^-_k, t)$, can be continuously estimated by

$$\begin{aligned}\widehat{L}^y(T^-_k, t) =& mH\ell \sinh(\ell(T^-_k - t))p^x_{\text{st}}(t) \\ &+ \cosh(\ell(T^-_k - t))L^y(t)\end{aligned} \tag{9}$$

2) From T^-_k to T^+_k: If the CoM height is constant and the ground is flat, the angular momentum about the next contact point will be equal to the angular momentum about the current stance leg,

$$\widehat{L}^y(T^+_k, t) = \widehat{L}^y(T^-_k, t); \tag{10}$$

see (3).

What's more, the swing foot before impact will become the stance foot after impact,

$$p^x_{\text{st}\to\text{CoM}}(T_k^+) = p^x_{\text{sw}\to\text{CoM}}(T_k^-). \tag{11}$$

3) From T_k^+ to T_{k+1}^-: Similar to (9), the Angular Momentum at the end of next step is

$$\widehat{L}^y(T_{k+1}^-, t) = mH\ell \sinh(\ell T) p^x_{\text{st}\to\text{CoM}}(T_k^+) + \cosh(\ell T)\widehat{L}^y(T_k^+, t) \tag{12}$$

Combining (9)-(12), we can decide the desired swing foot position at the end of the *current* step, given the value of desired angular momentum at the end of the *next* step,

$$p^{x\ \text{des}}_{\mathbf{sw}\to\mathbf{CoM}}(T_k^-, t) := \frac{L^{y\ \text{des}}(T_{k+1}^-) - \cosh(\ell T)\widehat{L}^y(T_k^-, t)}{mH\ell\sinh(\ell T)}. \tag{13}$$

C. Lateral Control

From (4), the time evolution of the angular momentum about the contact point is decoupled about the x- and y-axes. Therefore, once a desired angular momentum at the end of next step is given, Lateral Control is essentially identical to Longitudinal Control and (13) can be applied equally well in the lateral direction. **The question becomes how to decide on $\mathbf{L^{x\ des}(T_{k+1}^-)}$.**

For walking in place or walking with zero average lateral velocity, it is sufficient to obtain $L^{x\ \text{des}}$ from a periodically oscillating LIP model,

$$L^{x\ \text{des}}(T_{k+1}^-) = \pm\frac{1}{2}mHW\frac{\ell\sinh(\ell T)}{1+\cosh(\ell T)}, \tag{14}$$

where W is the desired step width. The sign is positive if next stance is left stance and negative if next stance is right stance. Lateral walking can be achieved by adding an offset to $L^{x\ \text{des}}$.

D. Turning

Turning in essence is changing direction of velocity. At turning, **same value** of $L^{x\ \text{des}}$ and $L^{y\ \text{des}}$ will be defined in **different frame** at each step, and the foot placement will be calculated correspondingly.

V. Implementing the LIP-based Angular Momentum Controller on a Real Robot

In this section we introduce the control variables for Cassie Blue and generate their reference trajectory. As in [7], we leave the stance toe passive. Consequently, there are nine (9) control variables, listed below from the top of the robot to the end of the swing leg,

$$h_0 = \begin{bmatrix} \text{torso pitch} \\ \text{torso roll} \\ \text{stance hip yaw} \\ \text{swing hip yaw} \\ p^z_{\text{st}\to\text{CoM}} \\ p^x_{\text{sw}\to\text{CoM}} \\ p^y_{\text{sw}\to\text{CoM}} \\ p^z_{\text{sw}\to\text{CoM}} \\ \text{swing toe absolute pitch} \end{bmatrix}. \tag{15}$$

For later use, we denote the value of h_0 at the beginning of the current step by $h_0(T_{k-1}^+)$. When referring to individual components, we'll use $h_{03}(T_{k-1}^+)$, for example.

We first discuss variables that are constant. The reference values for torso pitch, torso roll, and swing toe absolute pitch are constant and zero, while the reference for $p^z_{\text{st}\to\text{CoM}}$, which sets the height of the CoM with respect to the ground, is constant and equal to H.

We next introduce a phase variable

$$s := \frac{t - T_{k-1}^+}{T} \tag{16}$$

that will be used to define quantities that vary throughout the step to create "leg pumping" and "leg swinging". The reference trajectories of $p^x_{\text{sw}\to\text{CoM}}$ and $p^y_{\text{sw}\to\text{CoM}}$ are defined such that:

- at the beginning of a step, their reference value is their actual position;
- the reference value at the end of the step implements the foot placement strategy in (13); and
- in between a half-period cosine curve is used to connect them, which is similar to the trajectory of an ordinary (non-inverted) pendulum.

The reference trajectory of $p^z_{\text{sw}\to\text{CoM}}$ assumes the ground is flat and the control is perfect:

- at mid stance, the height of the foot above the ground is given by z_{CL}, for the desired vertical clearance.

The reference trajectories for the stance hip and swing hip yaw angles are simple straight lines connecting their initial actual position and their desired final positions. For walking in a straight line, the desired final position is zero. To include turning, the final value has to be adjusted. Suppose that a turn angle of ΔD_k^{des} radians is desired. One half of this value is given to each yaw joint:

- $+\frac{1}{2}\Delta D_k^{\text{des}} \to$ swing hip yaw; and
- $-\frac{1}{2}\Delta D_k^{\text{des}} \to$ stance hip yaw

The signs may vary with the convention used on other robots.

The final result for Cassie Blue is

$$h_{\text{d}}(s) := \begin{bmatrix} 0 \\ 0 \\ (1-s)h_{03}(T_{k-1}^+) + s(-\frac{1}{2}(\Delta D_k)) \\ (1-s)h_{04}(T_{k-1}^+) + s(\frac{1}{2}(\Delta D_k)) \\ H \\ \frac{1}{2}\left[(1+\cos(\pi s))h_{06}(T_{k-1}^+) + (1-\cos(\pi s))p^{x\ \text{des}}_{\text{sw}\to\text{CoM}}(T_k^-)\right] \\ \frac{1}{2}\left[(1+\cos(\pi s))h_{07}(T_{k-1}^+) + (1-\cos(\pi s))p^{y\ \text{des}}_{\text{sw}\to\text{CoM}}(T_k^-)\right] \\ 4z_{cl}(s-0.5)^2 + (H - z_{CL}); \\ 0 \end{bmatrix}. \tag{17}$$

When implemented with an Input-Output Linearizing Controller[1] so that h_0 tracks h_d, the above control policy allows Cassie to move in 3D in simulation. Figure 7 shows Cassie starts from a walking in place gait and accelerate to a speed of 2.8 m/s.

[1]The required kinematic and dynamics functions are generated with FROST [23].

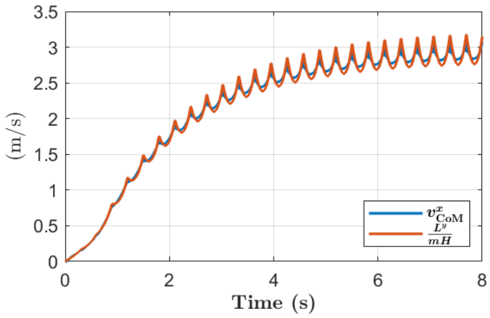

Fig. 7: Simulation results of Cassie. $\frac{L^{x \text{ des}}}{mH}$ ramped up from 0 to 3 m/s.

VI. Experimental Results

A description of a practical implementation of the controller is omitted here because of space limitations. A brief description can be found in [24]. Details of it will be included in a longer publication. The controller was implemented on Cassie Blue. The closed-loop system consisting of robot and controller was evaluated in a number of situations that are itemized below.

- **Walking in a straight line on flat ground.** Cassie could walk in place and walk stably for speeds ranging from zero to 2.1 m/s.
- **Diagonal Walking.** Cassie is able to walk simultaneously forward and sideways on grass, at roughly 1 m/s in each direction.
- **Sharp turn.** While walking at roughly 1 m/s, Cassie Blue effected a 90^o turn, without slowing down.
- **Rejecting the classical kick to the base of the hips.** Cassie was able to remain upright under "moderate" kicks in the longitudinal direction. The disturbance rejection in the lateral direction is not as robust as the longitudinal, which is mainly caused by Cassie's physical design: small hip roll motor position limits.
- **Finally we address walking on rough ground**. Cassie Blue was tested on the iconic Wave Field of the University of Michigan North Campus. The foot clearance was increased from 10 cm to 20 cm to handle the highly undulating terrain. Cassie is able to walk through the"valley" between the large humps with ease at a walking pace of roughly 0.75 m/s, without falling in all tests. The row of ridges running east to west in the Wave Field are roughly 60 cm high, with a sinusoidal structure. We estimate the maximum slope to be 40 degrees. Cassie is able to cross several of the large humps in a row, but also fell multiple times. On a more gentle, straight grassy slope of roughly 22 degrees near the laboratory, Cassie can walk up it with no difficulty whatsoever.

VII. Conclusions

We argued that a one-step ahead prediction of angular momentum about the contact point has many advantages for feedback control. While we only demonstrated this for step placement in a LIP-inspired controller, we believe the same will hold on many other control strategies.

Using our new controller, Cassie was able to accomplish a wide range of tasks with nothing more than common sense task-based tuning: a higher step frequency to walk at 2.1 m/s and extra foot clearance to walk over slopes exceeding 15 degrees. Moreover, in the current implementation, there is no optimization of trajectories used in the implementation on Cassie. The robot's performance is currently limited by the hand-designed trajectories leading to joint-limit violations and foot slippage. These limitations will be alleviated by incorporating optimization.

The current controller tries its best to maintain a zero center of mass velocity in the z-direction. This simplifies the transition formula for the angular momentum at impact. As in [14], it will be interesting to exploit changes in the vertical component of the center of mass velocity in order to better achieve a desired angular momentum.

(a) Fast Walking

(b) Rough Terrain

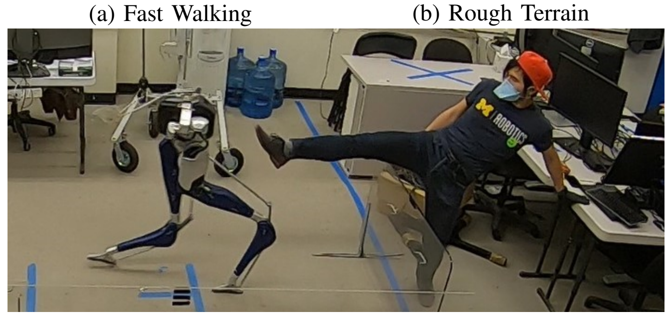

(c) Disturbance Rejection

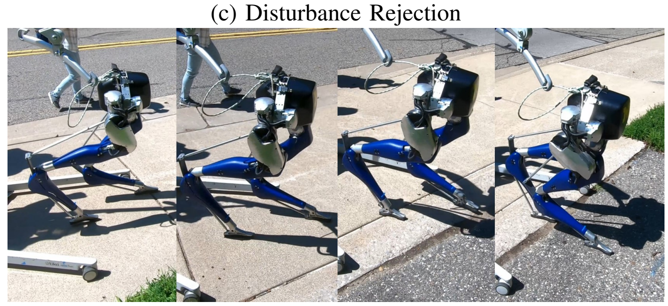

(d) A Fast 90 Degree Turn with a Long Stride

Fig. 8: Images from several closed-loop experiments conducted with Cassie Blue and the controller developed in this paper.Short Footage of those experiments are compiled in video [25]. Longer versions can be found in [26]

REFERENCES

[1] J. W. Grizzle, G. Abba, and F. Plestan. Asymptotically stable walking for biped robots: Analysis via systems with impulse effects. *IEEE Transactions on Automatic Control*, 46(1):51–64, January 2001.

[2] A. D. Ames, E. A. Cousineau, and M. J. Powell. Dynamically stable bipedal robotic walking with NAO via human-inspired hybrid zero dynamics. In *Proceedings of the 15th ACM international conference on Hybrid Systems: Computation and Control*, pages 135–144. ACM, 2012.

[3] Shuuji Kajita, Fumio Kanehiro, Kenji Kaneko, Kazuhito Yokoi, and Hirohisa Hirukawa. The 3d linear inverted pendulum mode: A simple modeling for a biped walking pattern generation. In *Proceedings 2001 IEEE/RSJ International Conference on Intelligent Robots and Systems. Expanding the Societal Role of Robotics in the the Next Millennium (Cat. No. 01CH37180)*, volume 1, pages 239–246. IEEE, 2001.

[4] Xingye Da, Omar Harib, Ross Hartley, Brent Griffin, and Jessy W Grizzle. From 2D design of underactuated bipedal gaits to 3D implementation: Walking with speed tracking. *IEEE Access*, 4:3469–3478, 2016.

[5] Ross Hartley, Xingye Da, and Jessy W. Grizzle. Stabilization of 3D underactuated biped robots: Using posture adjustment and gait libraries to reject velocity disturbances. In *IEEE Conference on Control Technology and Applications (CCTA)*, 2017.

[6] Omar Harib, Ayonga Hereid, Ayush Agrawal, Thomas Gurriet, Sylvain Finet, Guilhem Boeris, Alexis Duburcq, M. Eva Mungai, Matthieu Masselin, Aaron D. Ames, Koushil Sreenath, and Jessy Grizzle. Feedback control of an exoskeleton for paraplegics: Toward robustly stable hands-free dynamic walking. *arXiv preprint arXiv:1802.08322 [cs.RO]*, 2018.

[7] Y. Gong, R. Hartley, X. Da, A. Hereid, O. Harib, J. Huang, and J. Grizzle. Feedback control of a cassie bipedal robot: Walking, standing, and riding a segway. In *2019 American Control Conference (ACC)*, pages 4559–4566, 2019.

[8] Xingye Da and Jessy Grizzle. Combining trajectory optimization, supervised machine learning, and model structure for mitigating the curse of dimensionality in the control of bipedal robots. *The International Journal of Robotics Research*, 38(9):1063–1097, 2019.

[9] Jerry Pratt, John Carff, Sergey Drakunov, and Ambarish Goswami. Capture point: A step toward humanoid push recovery. In *2006 6th IEEE-RAS international conference on humanoid robots*, pages 200–207. IEEE, 2006.

[10] Johannes Englsberger, Christian Ott, Máximo A Roa, Alin Albu-Schäffer, and Gerhard Hirzinger. Bipedal walking control based on capture point dynamics. In *2011 IEEE/RSJ International Conference on Intelligent Robots and Systems*, pages 4420–4427. IEEE, 2011.

[11] S. Kajita, F. Kanehiro, K. Kaneko, K. Fujiwara, K. Harada, K. Yokoi, and H. Hirukawa. Biped walking pattern generation by using preview control of zero-moment point. In *2003 IEEE International Conference on Robotics and Automation (Cat. No.03CH37422)*, volume 2, pages 1620–1626 vol.2, 2003.

[12] R. Tedrake, S. Kuindersma, R. Deits, and K. Miura. A closed-form solution for real-time zmp gait generation and feedback stabilization. In *2015 IEEE-RAS 15th International Conference on Humanoid Robots (Humanoids)*, pages 936–940, 2015.

[13] Brent Griffin and Jessy Grizzle. Nonholonomic virtual constraints and gait optimization for robust walking control. *The International Journal of Robotics Research*, page 0278364917708249, 2016.

[14] Matthew J Powell and Aaron D Ames. Mechanics-based control of underactuated 3d robotic walking: Dynamic gait generation under torque constraints. In *2016 IEEE/RSJ International Conference on Intelligent Robots and Systems (IROS)*, pages 555–560. IEEE, 2016.

[15] JW Grizzle, Claude H Moog, and Christine Chevallereau. Nonlinear control of mechanical systems with an unactuated cyclic variable. *IEEE Transactions on Automatic Control*, 50(5):559–576, 2005.

[16] Eric R Westervelt, Christine Chevallereau, Jun Ho Choi, Benjamin Morris, and Jessy W Grizzle. *Feedback control of dynamic bipedal robot locomotion*. CRC press, 2007.

[17] J. Pratt and R. Tedrake. Velocity-based stability margins for fast bipedal walking. In Moritz Diehl and Katja Mombaur, editors, *Fast Motions in Biomechanics and Robotics*, volume 340 of *Lecture Notes in Control and Information Sciences*, pages 299–324. Springer Berlin Heidelberg, 2006.

[18] S. Kajita and K. Tani. Study of dynamic biped locomotion on rugged terrain-derivation and application of the linear inverted pendulum mode. In *Robotics and Automation, 1991. Proceedings., 1991 IEEE International Conference on*, pages 1405–1411 vol.2, 1991.

[19] M. H. Raibert. Hopping in legged systems—modeling and simulation for the two-dimensional one-legged case. *IEEE Transactions on Systems, Man and Cybernetics*, 14(3):451–63, June 1984.

[20] Miles A Townsend. Biped gait stabilization via foot placement. *Journal of biomechanics*, 18(1):21–38, 1985.

[21] Xiaobin Xiong and Aaron D Ames. Orbit characterization, stabilization and composition on 3d underactuated bipedal walking via hybrid passive linear inverted pendulum model. In *2019 IEEE/RSJ International Conference on Intelligent Robots and Systems (IROS)*, pages 4644–4651. IEEE, 2019.

[22] C. Chevallereau, G. Abba, Y. Aoustin, F. Plestan, E. R. Westervelt, C. Canudas-de-Wit, and J. W. Grizzle. RABBIT: A testbed for advanced control theory. *IEEE Control Systems Magazine*, 23(5):57–79, October 2003.

[23] Hereid Ayonga. Fast Robot Optimization and Simulation Toolkit(FROST. https://ayonga.github.io/frost-dev/.

[24] Yukai Gong and Jessy Grizzle. Angular momentum about the contact point for control of bipedal locomotion: Validation in a lip-based controller. *arXiv preprint arXiv:2008.10763 [cs.CV]*, 2020.

[25] Experiment Video Compilation. https://youtu.be/V36DCsc6iio.

[26] Michigan Robotics: Dynamic Legged Locomotion Lab Youtube Channel. https://www.youtube.com/channel/UCMfDV8rkQqWhUwnTAYAq0tQ. Accessed: 2019-01-31.